Catena 157 (2017) 279–285

Contents lists available at ScienceDirect

Catena

journal homepage: www.elsevier.com/locate/catena

Developing equations to explore relationships between aggregate stability and erodibility in Ultisols of subtropical China

Hai Xiao[a], Gang Liu[a,b,*], Puling Liu[a,b], Fenli Zheng[a,b], Jiaqiong Zhang[a,b], Feinan Hu[a,b]

[a] State Key Laboratory of Soil Erosion and Dryland Farming on the Loess Plateau, Institute of Soil and Water Conservation, Northwest A & F University, Yangling 712100, People's Republic of China

[b] Institute of Soil and Water Conservation of Chinese Academy of Sciences and Ministry of Water Resources, Yangling 712100, People's Republic of China

ARTICLE INFO

Keywords:
REE
Rill and interrill erosion
Soil erodibility
Aggregate stability
WEPP model

ABSTRACT

A soil aggregate represents a key soil structural unit that influences several physical soil properties such as water infiltration, runoff and erosion. The relationships between soil aggregate stability and interrill and rill erodibility are critical to process-based erosion prediction models yet remain unclear, likely due to the difficulty of distinguishing between interrill and rill-eroded sediment during the erosion process. This study was designed to partition interrill and rill erosion rates and relate them to the aggregate stability of Ultisols in subtropical China. Six kinds of rare earth elements (REEs) were applied as tracers mixed with two cultivated soils developed over Quaternary red clay or shale at six slope positions. Soil aggregate stability was determined by the Le Bissonnais (LB)-method. Simulated rainfall of three intensities (60, 90 and 120 mm h^{-1}) was applied to a soil plot (2.25 m long, 0.5 m wide, 0.2 m deep) at three slope gradients (10°, 20° and 30°) for a duration of 30 min after runoff initiation. The results indicated that rill and interrill erosion rates in the soil developed over shale were considerably greater than those in the soil developed over Quaternary red clay. Equations using an aggregate stability index A_s to replace the erodibility factor of interrill and rill erosion in the Water Erosion Prediction Project (WEPP) model were constructed after analysing the relationships between estimated and measured rill and interrill erosion data. The results show that these equations based on A_s have the potential to improve methods for assessing interrill and rill erosion erodibility synchronously for subtropical Ultisols by using an REE tracing method.

1. Introduction

Ultisols, locally known as red soils, occupy approximately 1.14 million km^2 of southeastern China. Improper land use and poor soil management have caused severe soil losses from water erosion in the region (Liang et al., 2010) resulting in the complete loss of the A and/or B horizons, and leaving the plinthic C horizon exposed in numerous areas of southern China (Deng et al., 2010).

Process-based erosion models applied to agricultural soils usually rely on the rill-interrill concept, which requires different relationships and algorithms (Nearing et al., 1989; Laflen et al., 1991) for each component. Rill erosion occurs due to the detachment and transportation of particles and aggregates by concentrated flow, whereas interrill erosion occurs between rills because of the combined effects of raindrop impact and shallow overland flow. Soil erosion prediction is a complex process affected by several factors. Soil erodibility, K_i for interrill erosion and K_r for rill erosion, is regarded as a key parameter for evaluating a soil's susceptibility to erosion and is essential for predicting soil loss and evaluating the environmental effects thereof (Wang et al., 2013). Both K_i and K_r can be determined either by data from experimental plots (Truman and Bradford, 1995; Zhang et al., 2003; Wang et al., 2012) or from soil properties, including soil texture, cohesion strength, soil shear strength, clay content and aggregate stability (Wang et al., 2013).

Among the aforementioned properties, aggregate stability, is a key soil structural trait that describes the resistance of aggregates to the disintegrating action of water (Valmis et al., 2005). Aggregate stability has an enormous influence on soil erosion (Barthès and Roose, 2002; Dimoyiannis et al., 2006; Ding and Zhang, 2016). For instance, rill erosion in soils with large aggregate stability is less than that in soils with low aggregate stability (Zheng et al., 1989). The ability of topsoil aggregates to resist erosion is reportedly a valuable indicator of field-assessed runoff and interrill erosion of sandy loam soils (Cantón et al., 2009). Previous studies have established formulas to describe the relationship between interrill erosion and topsoil aggregate stability, which is reflected through different indicators, such as percolation

* Corresponding author at: No. 26, Xinong Road, Yangling, Shaanxi Province 712100, People's Republic of China.
E-mail address: gliu@foxmail.com (G. Liu).

http://dx.doi.org/10.1016/j.catena.2017.05.032
Received 25 April 2016; Received in revised form 20 May 2017; Accepted 24 May 2017

stability (*PS*) (Mbagwu and Auerswald, 1999) and aggregate instability (β) (Valmis et al., 2005; Dimoyiannis et al., 2006). Both *PS* and β mainly simulate the fast wetting effect, which is a major influence on aggregate destruction. These parameters can partially explain the relationship between interrill erosion and topsoil aggregate stability. However, the mechanisms primarily responsible for aggregate breakdown during water erosion processes include both slaking by fast wetting and mechanical breakdown due to raindrop impact (Shi et al., 2012). Mechanical breakdown due to raindrop impact is another important sub-process of interrill erosion.

The stability index, A_s, is probably a better aggregate indicator for slaking by fast wetting and mechanical breakdown due to raindrop impact effects (Yan et al., 2008; Shi et al., 2010). A_s was used by Yan et al. (2008) and Shi et al. (2010) to replace K_i in the interrill erosion equation of the Water Erosion Prediction Project (WEPP) model. Wang et al. (2012) discovered that A_s was also closely related to the soil detachment rate and was linearly correlated with the concentrated flow erodibility factor (K_r) under scouring conditions ($R^2 = 0.70$, $p < 0.01$). That study proposed using A_s to in place of K_r in the rill erosion equation of the WEPP model. Thus, A_s can be used to express both K_i in the interrill erosion equation and K_r in the rill erosion equation of the WEPP model. However, interrill and rill erosion are continual and simultaneous processes on slopes with rill present (Song et al., 2003). For the purposes of accurately describing the erosion process and calculating the relative contributions of interrill and rill erosion, it is necessary to determine the relationships between K_i, K_r and A_s simultaneously during rainstorms.

Conventional erosion monitoring techniques such as field plots (Stefano et al., 2013) and stereo-photo-surveys (Nachtergaele and Poesen, 1999), cannot readily distinguish between interrill- and rill-eroded sediments. Numerous methods have been applied in recent decades for distinguishing interrill- and rill- eroded sediments in experimental plots using tracers, e.g., beryllium-7 (Yang et al., 2006; Liu et al., 2011), glass particles (Young and Holt, 1968), artificial radionuclides (^{134}Cs & ^{60}Co) (Greenwood, 2012) and REEs (Zhang et al., 2001; Song et al., 2003; Liu et al., 2004). The exact proportion of the fallout beryllium-7 inventory that reaches the soil surface can be greatly spatially variable due to uptake by vegetation, which is highly variable and depends on vegetation density and length (Mabit et al., 2008; Greenwood et al., 2014). Fluorescent dyes incorporated into glass particles have previously been used in soil erosion studies (Young and Holt, 1968). However, glass particles differ in their size distribution, particle density, shape, surface morphology and surface chemical properties from soil particles and aggregates such that they may not bind well to the soil particles and aggregates and therefore get transported separately (Zhang et al., 2001). REEs are found at low background concentrations in soils, chemically stable, environmentally safe and undergo low plant uptake. REEs therefore make ideal soil tracers because they also strongly adsorb to soil particles without interfering in their movement and can be analysed readily and accurately (Mahler et al., 1998; Zhang et al., 2001). They have been widely applied in research on erosion processes, particularly for tracing sediment sources and sediment movement from slopes and watersheds (Tian et al., 1994; Matisoff et al., 2001; Song et al., 2003; Liu et al., 2004; Kimoto et al., 2006; Polyakov and Nearing, 2004; Polyakov et al., 2009; Liu et al., 2016a, 2016b). Since interrill erosion generally occurs from the upper 10 mm of soil (Xue et al., 2004; Liu et al., 2011; Greenwood, 2012), REEs applied at different depths have the potential to distinguish interrill and rill erosion during rainstorms K_i and K_r can then be estimated simultaneously.

Against this background information, the purposes of this study were (i) to partition interrill and rill erosion for Ultisols using REEs as tracers during simulated rainstorms; (ii) to develop new equations for predicting both interrill and rill erosion rates that incorporate relevant soil aggregate stability indices to replace the erodibility factors; and (iii) to validate the newly developed equations.

2. Materials and methods

2.1. Study area

Soils developed over Quaternary red clay or shale, classified as Ultisols (Soil Survey Staff, 2014), were collected from Xianning County (29°39′–30°02′ N and 114°06′–114°43′ E) and Yidu City (30°05′–30°35′ and 110°05′–111°35′ E). Xianning and Yidu are located in the southeast and southwest of Hubei province, China, respectively, and are characterized as having a subtropical monsoon climate. The annual average precipitation and temperature in Xianning and Yidu are 1577 mm and 16.8 °C and are 1600 mm and 16.7 °C, respectively. Rainfall intensities exceeding 50 mm h^{-1} in this area are common (Shi et al., 2010). Samples collected from the uppermost 30-cm layer comprise 58.3% clay, 32.5% silt and 9.2% sand for the soil developed over Quaternary red clay (clay soil) and 21.5% clay, 38.3% silt and 40.2% sand for the soil developed over shale (loam soil). The bulk density and organic matter content for soil developed over Quaternary red clay were 1.16 g cm^{-3} and 1.5%, respectively, and 1.25 g cm^{-3} and 1.7% for soil developed over the shale.

2.2. Experimental design

All soil samples used in the experiment were air-dried and screened through a 2-mm sieve. Six REE oxides in powder form (Yb_2O_3, Tb_4O_7, Sm_2O_3, CeO_2, La_2O_3, Dy_2O_3) were chosen for this study based on their price, quantity to be applied, and susceptibility to detection (Xue et al., 2004). The concentrations of the background and applied REEs in the experiment are shown in Table 1.

Each REE oxide was initially mixed thoroughly with 1 kg of air-dried soil and then mixed with additional air-dried soil approximately five times until it reached the target application concentration. Soil samples, each containing a corresponding REE, were prepared for packing into metal plots with dimensions measuring 2.25 m in length, 0.5 m in width, and 0.2 m in depth as depicted in Fig. 1. The plot was subdivided into three equal parts of length 75 cm each. The plots were set at 10°, 20° and 30°. Packing was carried out layer by layer to achieve the desired uniform mean bulk density (1.16 g cm^{-3} for the soil developed over Quaternary red clay and 1.25 g cm^{-3} for the soil developed over shale). Erosion within the depths of 0.0–1.0 cm and 1.0–20.0 cm was deemed to be interrill and rill erosion, respectively (Xue et al., 2004; Liu et al., 2011; Greenwood, 2012). Thus, six areas with different REEs were existing as shown in Fig. 1. The bottoms of the plots were perforated and covered with a 20 cm layer of sand to facilitate even drainage of percolating soil water. Runoff was funnelled to a collection vessel placed at the lower end of the plot. After packing, the surface soil was watered to saturation, covered with a rain shelter and maintained for three days without any disturbance to enhance the adsorption of the REEs to soil particles.

Three rainfall simulations, with intensities of 60, 90 and 120 mm h^{-1}, were conducted for 30 min following the initiation of runoff. These intensities were based on the natural maximum rainfall

Table 1
Background and applied REEs concentrations in the experiment.

Element	La_2O_3	CeO_2	Sm_2O_3	Tb_4O_7	Ho_2O_3	Yb_2O_3
Background concentration in the soil developed over Quaternary red clay (mg·kg^{-1})	25.86	49.42	1.73	0.45	0.42	1.29
Background concentration in the soil developed over shale (mg·kg^{-1})	15.46	32.66	2.48	0.31	0.31	0.93
Applied concentration (mg·kg^{-1})	773.00	489.90	124.00	11.63	18.60	18.60

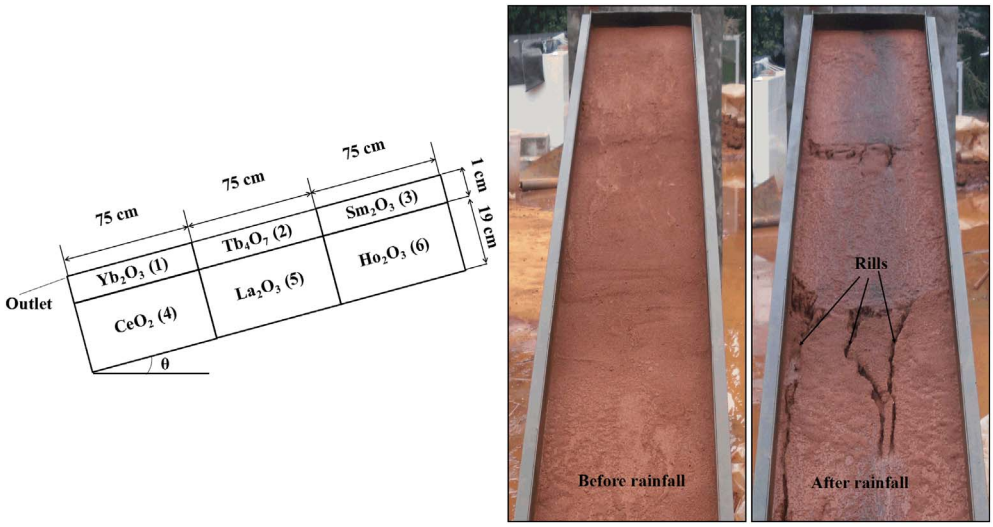

Fig. 1. Schematic representation of REE oxides distribution. Yb_2O_3 is REE oxide powder, (1) is area number; θ is gradient.

intensity occurring for 30-min duration with return periods of 2, 5 and 20 years near Xianning County and Yidu City (Hu et al., 2016). In total, there were 18 treatments, comprising three slope gradients (10°, 20° and 30°), three rainfall intensities (60, 90 and 120 mm h^{-1}), and two soil types (soil developed over Quaternary red clay and shale). Each treatment was performed in triplicate; therefore, a total of 54 rainfall simulations were carried out in this study. Runoff and sediments were collected in a series of plastic containers at 3 min intervals over the 30 minute period. The volume of water in each container was measured, and the sediment was air dried and weighed.

2.3. Laboratory analysis

A modified standard methodology for extracting metals from environmental samples (US EPA, 1995) was used to extract the REE from the various soil-REE mixtures and sediment samples in a sequence that combined ten steps. (1) A 50 g sample of the air-dried soils was taken and ground to pass through a 0.15 mm (100 meshes) sieve. (2) Two replicate 25 mg subsamples of the sieved sample were used for analysis of the REE contents; each 25-mg subsample was placed in a 20 ml polytetrafluoroethylene (PTFE) cylindrical flask. (3) 0.5 ml of concentrated HNO_3 (Guarantee Reagent (GR), 68% by weight) and 1 ml concentrated HF (GR, 40% by weight) were added to the subsample. (4) The flask was covered by a tightly fitting lid and the flask was then sealed into a tightly fitting steel sheath before heating at 185 °C in an oven for 24 h. (5) The flask was cooled to room temperature, the lid was removed, and the open flask was then heated at 130 °C on an electric hot plate until the subsample was almost dry. (6) 1 ml of concentrated HNO_3 (GR, 68% by weight) was added and the suspension was heated as in step 5 until the sample was almost dry. (7) Another 1 ml of concentrated HNO_3 (GR, 68% by weight) was added and the suspension was heated as in step 5 until the sample was almost dry. (8) 5 ml of HNO_3 (GR, 68% by weight) solution (1:1 in volume) was added to the flask, the lid was tightened, and the sealed flask was put into the steel sheath and heated at 130 °C in an oven for 3 h. (9) The flask was cooled to room temperature and the suspension was transferred to a 50-ml volumetric flask in which the volume was made up to 50 ml with deionized water (18 MΩ·cm^{-1}). (10) The volumetric flask was shaken well, and the suspension was transferred to a 10-ml polyethylene centrifuge tube and centrifuged to obtain clear extracts for REE determination. Mean values of the two subsamples (replicates) were calculated for all of the REE analyses.

Inductively Coupled Plasma Mass Spectrometry (X Series 2 ICP-MS, Thermo Fisher Scientific, US) analysis of the extracts containing REEs was carried out at China Three Gorges University. A stock internal standard solution containing Rh and Re (10 μg·l^{-1}) was added in the analysis process for analytical quality control. Three separate measurements were taken for each extract and the mean value of the measurements was calculated.

The LB-method proposed by Le Bissonnais (1996) was used to measure aggregate stability for the investigation of the following breakdown mechanisms: fast wetting (FW); slow wetting (SW); and mechanical breakdown by stirring pre-wetted aggregates (WS). Using a small spoon to take 5 g of air-dried aggregates of 3–5 mm in diameter which was obtained by dry sieving and oven-dried at 40 °C for 24 h with three times random selected. Aggregates were gently immersed in distilled water and the water vacuumed off after 10 min in FW treatment. For SW treatment, aggregates were placed on a filter-paper for 30 min, and subjected to a tension of 0.3 kPa. For WS treatment, aggregates were immersed in ethanol (95% in mass) for 10 min and transferred to a 500 ml flask with 200 cm^3 deionized water then corked and agitated up and down 20 times for 1 min then allowed to settle for 30 min. The corresponding aggregates were transferred to a 0.05 mm sieve immersed in ethanol (95% in mass) and gently moved up and down (2 cm in height) 20 times by hand. The remaining aggregates on the 0.05 mm sieve were collected and measured for their size distribution by dry sieving through 3.0, 2.0, 1.0, 0.5, 0.2, 0.1 and 0.05 mm pore openings after drying in an oven at 40 °C for 48 h. Each treatment was replicated 3 times.

2.4. Calculation

The mass of soil loss from section j (j = 1, 2, 3 … 6) in the plot can be calculated using Eq. (1):

$$w_j = \frac{(R_j - B_j) \times W}{C_j} \quad (1)$$

where w_j is the mass of soil loss in section j (kg); R_j is the actual measured concentration of REEs in section j of the sediment samples (mg·kg^{-1}); B_j is the background concentration of REEs in section j (mg·kg^{-1}); W is the mass of the sediment samples (kg) and C_j is the applied concentration of REEs in section j (mg·kg^{-1}). The relative contribution of each section (r_j) is given Eq. (2):

$$r_j = \frac{w_j}{W} \quad (2)$$

Aggregate stability for each sample was expressed in terms of the mean weight diameter for the different size classes calculated using Eq. (3):

$$MWD = \sum_{i=1}^{n} \overline{x_i} w_i \tag{3}$$

where w_i is the weight fraction of aggregates in the size class i with an average diameter x_i.

The relative slaking index (*RSI*) and the relative mechanical breakdown index (*RMI*) were used to determine the resistance to slaking and the mechanical breakdown of the soils, respectively. And A_s is the stability index in this research.

$$RSI = \frac{MWD_{sw} - MWD_{fw}}{MWD_{sw}} \tag{4}$$

$$RMI = \frac{MWD_{sw} - MWD_{ws}}{MWD_{sw}} \tag{5}$$

$$A_S = RSI \times RMI \tag{6}$$

where MWD_{fw}, MWD_{ws}, and MWD_{sw} are the mean weight diameter obtained by the FW, WS, and SW treatments, respectively.

Runoff shear stress (τ) can be estimated using Eq. (7) (Guo et al., 2013):

$$\tau = \phi \mathrm{gHS} \tag{7}$$

where φ is the water mass density (kg m^{-3}); g is the gravity constant (m s^{-2}); S is the slope gradient (m m^{-1}); H (m) is the mean flow depth calculated by Eq. (8):

$$H = Q/\mathrm{B}v \tag{8}$$

where Q is the flow rate (m^3 s^{-1}); B is the width of the flow cross-section (m); v is the flow velocity (m s^{-1}) measured by ink dye technique (Zhang et al., 2010) and was multiplied by a correction factor of 0.67 for amendment as the measured surface flow velocity was larger than the mean flow velocity (Li et al., 1996).

The interrill and rill erosion rates equation in WEPP model are as follows (Nearing et al., 1989; Flanagan and Nearing, 1995):

$$D_i = K_i S_f I^2 \tag{9}$$

$$D_r = K_r(\tau - \tau_c) \tag{10}$$

where D_i is the interrill erosion rate (kg m^{-2} s^{-1}); K_i is the interrill soil erodibility (kg m^{-2} mm^{-1}); I is the rainfall intensity rate (mm s^{-1}); D_r is the rill detachment rate (kg m^{-2} s^{-1}); K_r is rill soil erodibility (s m^{-1}); τ is the flow shear stress acting on the soil (Pa); τ_c is the critical shear stress of the soil (Pa); S_f is an interrill slope steepness factor which can be estimated by (Liebenow et al., 1990):

$$S_f = 1.05 - 0.85e^{-4\sin\theta} \tag{11}$$

where θ is the slope angle.

As mentioned above, the stability index (A_s) may have the potential to express K_i in interrill erosion equation and K_r in rill erosion equation in the WEPP model synchronously. So we make an assumption that D_i and D_r can be calculated by the following equations:

$$D_i = aA_s S_f I^2 \tag{12}$$

$$D_r = bA_s(\tau - \tau_c) \tag{13}$$

where a and b are coefficients.

3. Results

3.1. Interrill and rill erosion

Interrill and rill erosion increased with increasing rainfall intensity and slope gradient for both soils (Fig. 2). Both the rill erosion and interrill erosion of the soil developed over shale were considerably higher than those of the soil developed over Quaternary red clay, indicating that the former soil type can be more easily detached and transported by both interrill and rill erosion under the same conditions.

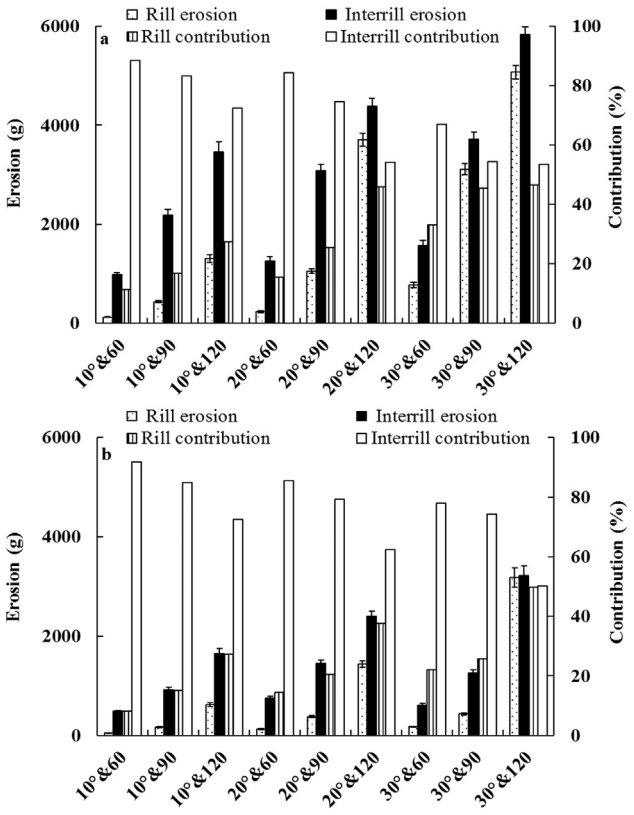

Fig. 2. Amount and contribution rate of rill and interrill erosion in different slope gradients and rainfall intensities (a is the soil developed over shale, b is the soil developed over Quaternary red clay, 10°&60 is 10° with rainfall intensity of 60 mm h^{-1}).

All contribution rates of interrill erosion to total soil loss were higher than 50%, and most were higher than 70% for the soil developed over Quaternary red clay. The rill erosion contribution increased with increasing rainfall intensity and slope gradient for both soils.

For interrill areas, the mean percentage contributions of the erosion from the downslope area (area 1), mid-slope area (area 2) and up-slope area (area 3) to total erosion for the soils developed over Quaternary red clay and shale were 41.33%, 42.21%and 27.53% and 23.55%, 6.62% and 4.52%, respectively (Fig. 3). The mean percentage of the erosion from interrill areas followed the ordering of, area 1 > area 2 > area 3; the area 3 erosion percentage of total erosion was much lower than those of the other two areas (areas 1 and 2) (Fig. 3). This result was consistent with those from previous studies by Tian et al. (1994) and Zhu et al. (2011). Rill erosion was rare under gentle slope and low rainfall intensity conditions, and mainly occurred on the downslope area (area 4), as evidenced by the area's much larger contribution percentage of the total relative to the other two areas (areas 5 and 6).

3.2. The stability index

The aggregate stability values of the soils developed over Quaternary red clay and shale calculated by Eqs. (3)–(6) are shown in Table 2. The values of MWD_{fw}, MWD_{ws} and MWD_{sw} for the soil developed over shale were lower than those for the soil developed over Quaternary red clay, indicating that the aggregate in the soil developed over Quaternary red clay was more stable than that in the soil developed over shale. In both types of soil, the values of aggregate stability could be ordered as $MWD_{fw} < MWD_{ws} < MWD_{sw}$ for the three treatments, suggesting that slaking (FW) is the most effective mechanism for aggregate breakdown, followed by mechanical breakdown (WS); chemical dispersion (SW) is the weakest breakdown mechanism. The *RSI* and *RMI* of the soil developed over shale were

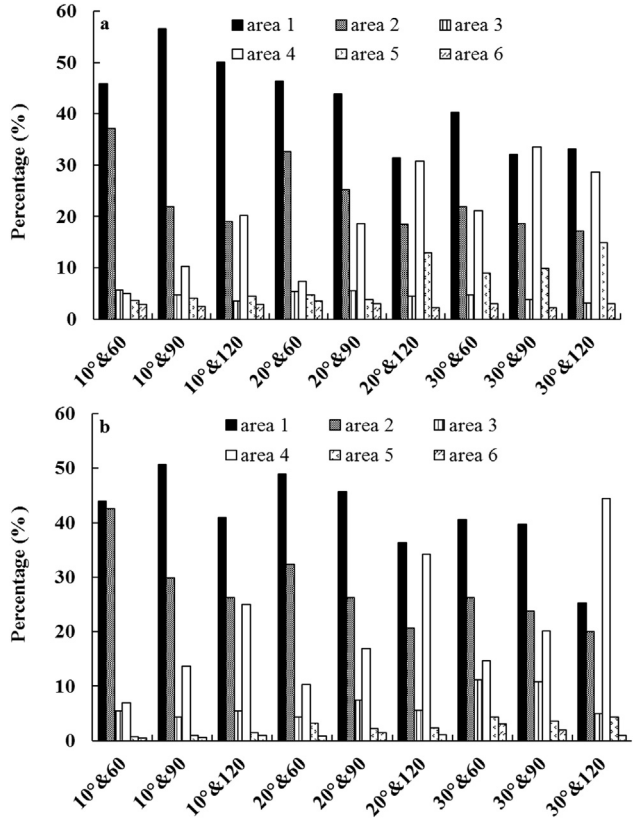

Fig. 3. Percentage rate of each area in different slope gradients and rainfall intensities (a is the soil developed over shale, b is the soil developed over Quaternary red clay, 1 is area number, 10° & 60 is 10° with rainfall intensity of 60 mm h^{-1}).

higher than those of the soil developed over Quaternary red clay (Table 2). Higher *RSI* and *RMI* of aggregates imply greater susceptibility to slaking and mechanical breakdown, respectively (Zhang and Horn, 2001). The A_s of the soil developed over shale was greater than that of the soil developed over Quaternary red clay, indicating that the former had a greater potential for detachment during both interrill and rill erosion (Yan et al., 2008; Wang et al., 2012).

3.3. Establishment of predict equations

The aggregate stability index A_s reflects soil resistance to both raindrop impact during interrill erosion and runoff shear stress impact during rill erosion. Based on data from thirty events selected at random, Fig. 4 presents the results of a linear regression analysis with a zero intercept for the measured and estimated interrill and rill erosion rates calculated using Eqs. (12) and (13) with coefficient set to values a and $b = 1$, respectively. The relationships indicate that coefficient values a and b should be 2.59 and 6.12, respectively (Fig. 4). Therefore, the interrill and rill erosion rates for the soils developed over Quaternary red clay and shale can be individually estimated by using the following equations:

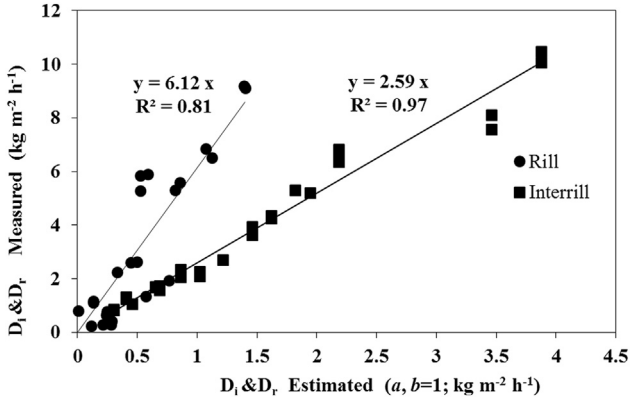

Fig. 4. Linear regressions with zero intercept between measured and estimated values of interrill and rill erosion rate using Eqs. (12) and (13) when the coefficients value a and $b = 1$ for both the soils developed over Quaternary red clay and shale, respectively.

$$D_i = 2.59 A_s S_f I^2 \quad (n = 30, R^2 = 0.97, p < 0.01) \tag{14}$$

$$D_r = 6.12 A_s (\tau - \tau_c) \quad (n = 30, R^2 = 0.81, p < 0.01) \tag{15}$$

3.4. Validation of the equations

The remaining interrill ($n = 24$) and rill erosion data ($n = 24$) were used for model validation. Fig. 5 illustrates moderate to good relationships between measured and predicted (using Eqs. (14) and (15)) values of interrill and rill erosion rates ($R^2 = 0.95$ and 0.76, respectively). The R^2 value for the validation of Eq. (15) is not as high as that for Eq. (14). Nevertheless, the results show that Eqs. (14) and (15) are effective for predicting interrill and rill erosion rates simultaneously during rainstorms.

4. Discussion

The aggregate in the soil developed over Quaternary red clay was more stable than that in the soil developed over shale, potentially because the clay content in the soil developed over shale was much lower than that in the soil developed over Quaternary red clay. Both clay and organic matter content can affect aggregate stability (Six et al., 2004; Wang et al., 2016). However, the nearly 70% increase of soil aggregate stability could be explained by the increase of clay content when organic C content was low (Le Bissonnais et al., 2007). Thus, the slightly higher organic matter content in the soil developed over shale relative to that in the soil developed over Quaternary red clay did not lead to more stable aggregates, because a simultaneous decrease of clay content overcompensated this effect. In this study, slaking (FW) has the greatest effect on aggregate breakdown, followed by mechanical breakdown (WS), whereas the chemical dispersion (SW) effect is the weakest of the breakdown mechanisms. This result was in line with previous studies undertaken on the same types of red soils (Yan et al., 2008; Shi et al., 2010; Wang et al., 2012). Chaplot et al. (2007) found that mechanical breakdown (wet-stirring treatment) resulted in the lowest aggregate stability among the three treatments, probably due to the high clay, iron and/or aluminium content in Ultisols and Alfisols from

Table 2
Aggregate stabilities measured by the LB-method on the soils developed over Quaternary red clay and shale.

Soil	MWD_{fw} (mm)	MWD_{ws} (mm)	MWD_{sw} (mm)	*RSI*	*RMI*	A_s
The soil developed over Quaternary red clay	0.72 ± 0.06a	2.24 ± 0.09a	2.74 ± 0.04a	0.737	0.182	0.135
The soil developed over shale	0.62 ± 0.04b	1.64 ± 0.13b	2.63 ± 0.10b	0.764	0.376	0.288

MWD_{fw}, MWD_{ws} and MWD_{sw} denote the mean weight diameters obtained after the fast-wetting (FW), pre-wetting and stirring (WS) and slow wetting (SW), respectively; RSI, RMI and A_s denote relative slaking index; relative mechanical breakdown index; aggregate stability index. Different letters in the same column mean significant difference between two sets of triplicate values at 0.05 level.

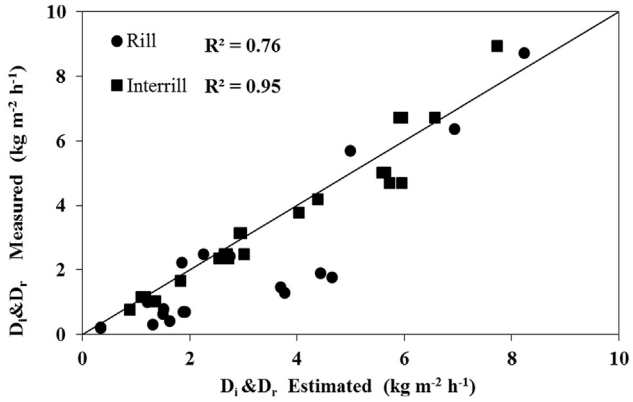

Fig. 5. Relationship between measured and estimated rate of interrill and rill erosion for validating.

tropical Northern Laos. Twelve soils in the Oceanic zone of the French Pyrenean have also been tested; either a wet-stirring treatment or a slow-wetting treatment may have the greatest impact on aggregate stability among the three treatments on these soils (Le Bissonnais and Arrouays, 1997).

The value of coefficient a in Eq. (15) was approximately 11 times greater than the corresponding a value of 0.23 from the Yan et al. (2008) study. This difference may be ascribed to the lack of rills in that study, as opposed to their presence in our study. Materials detached by rainsplash during interrill erosion can be transported merely by the rainsplash or by interrill shallow flow on slopes when rills are absent. However, when rills are present, much of the eroded material from interrill erosion area can be delivered into rill systems. The concentrated flow in rills has higher transport capacity than rainsplash and shallow flow (Liu et al., 2011). Therefore, this could result in a larger interrill erosion rate and correspondingly, a higher value for the coefficient a.

Linear relationships have previously been established between shear stress and soil detachment rate during concentrated flow (Zhang et al., 2003; Wang et al., 2012). However, these relationships can only describe the flow shear forces on surface soil; other processes occurring during rill erosion, such as side wall failure, headcut retreat and plunge pool dynamics, have not previously been taken into account (Wirtz et al., 2013). These sub-processes commonly occur during the rill development process and they likely account for a large proportion of rill erosion (Stefanovic and Bryan, 2009). In our study, Eq. (15) includes all sub-processes during rill development, which may be the reason why the R^2 for Eq. (15) is not as high as that for Eq. (14).

Our results show that it is possible to estimate interrill and rill erodibility simultaneously on the basis of aggregate stability measurements and an REE tracing method. The REE tracing method has been successfully applied in soil erosion investigations in numerous other areas (Zhang et al., 2001; Matisoff et al., 2001; Liu et al., 2004; Kimoto et al., 2006; Wang et al., 2008); therefore Eqs. (12) and (13) have the potential to be applied over a wider range of soil types. In addition, a more accurate method to detect different sub-processes in rill erosion and rill morphology is necessary for the purpose of improving prediction accuracy and simulating rill erosion processes in detail.

5. Conclusions

(i) Our results show that it is possible to estimate interrill and rill erodibility simultaneously on the basis of aggregate stability measurements using the REE tracing method. Both the rill erosion and interrill erosion of the soil developed over shale were considerably higher than those of the soil developed over Quaternary red clay. The mean percentage of the erosion from interrill areas followed the ordering of downslope area, mid-slope area and up-slope area. (ii) The equations incorporating the stability index, A_s, reliably reflect the soil interrill and rill erosion rates. Two equations using an aggregate stability index, A_s, were constructed to replace the erodibility factors, K_i and K_r for interrill and rill erosion, respectively, in the WEPP model. (iii) Two newly developed equations were subsequently verified.

The equations developed herein have great potential to be applied to a wider range of soil types. As our results are based on experiments on only two soils, future studies should investigate a wider range of soil types with various aggregation characteristics under more varied rainfall conditions in order to support the results obtained herein.

Acknowledgment

We thank Dr. Glenn Wilson for his suggestions and improving the English writing of the manuscript. This research was jointly supported by the Natural Science Basic Research Plan in Shaanxi Province of China (No. 2016JQ4017), the National Key Technology Research and Development Program of the Ministry of Science and Technology of China (No. 2015BAC01B03-03), the Natural Science Foundation of China (41201270, 41371281), the West Light Foundation of The Chinese Academy of Sciences (No. 2014-91), the Talents Research Start-up Foundation of Shaanxi Province (No. 2013-02100-Z111021512), the Chinese Universities Scientific Fund (No. 2452016102), and the Special-Funds of Scientific Research Programs of State Key Laboratory of Soil Erosion and Dryland Farming on the Loess Plateau (No. A314021403-C2). The authors also thank the three reviewers of the original manuscript for their insightful comments.

References

Barthès, B., Roose, E., 2002. Aggregate stability as an indicator of soil susceptibility to runoff and erosion: validation at several levels. Catena 47, 133–149.
Cantón, Y., Solé-Benet, A., Asensio, C., Chamizo, S., Puigdefábregas, J., 2009. Aggregate stability in range sandy loam soils relationships with runoff and erosion. Catena 77, 192–199.
Chaplot, V., Khampaseuth, X., Valentin, C., Le Bissonnais, Y., 2007. Interrill erosion in the sloping lands of northern Laos subjected to shifting cultivation. Earth Surf. Process. Landf. 32, 415–428.
Deng, H., Zhang, B., Yin, R., Wang, H.L., Mitchell, S.M., Griffiths, B.S., Daniell, T.J., 2010. Long-term effect of re-vegetation on the microbial community of a severely eroded soil in sub-tropical China. Plant Soil 328, 447–458.
Dimoyiannis, D., Valmis, S., Danalatos, N.G., 2006. Interrill erosion on cultivated Greek soils: modeling sediment delivery. Earth Surf. Process. Landf. 31, 940–949.
Ding, W.F., Zhang, X.C., 2016. Evaluation on using soil aggregate stability as an indicator of interrill erodibility. J. Mt. Sci-Engl. 13 (5), 831–843.
Flanagan, D.C., Nearing, M.A., 1995. USDA-Water Erosion Prediction Project, July 1995. NSERL Report No. 10. USDA-ARS National Soil Erosion Research Laboratory, West Lafayette, Ind.
Greenwood, P., 2012. Tracing fine-sediment using artificial radionuclides. In: Clarke, L.E., Nield, J.M. (Eds.), Geomorphological Techniques, Chapter 3, Section 5.2. British Society for Geomorphology, London, UK, pp. 1–10.
Greenwood, P., Walling, D.E., Quine, T.A., 2014. Using caesium-134 and cobalt-60 as tracers to assess the remobilization of recently-deposited overbank-derived sediment on river floodplains during subsequent inundation events. Earth Surf. Process. Landf. 39, 228–244.
Guo, T.L., Wang, Q.J., Li, D.Q., Zhuang, J., Wu, L.S., 2013. Flow hydraulic characteristic effect on sediment and solute transport on slope erosion. Catena 107, 145–153.
Hu, C.Q., Tong, Q., Fang, Y., Liu, J., Wu, L.X., 2016. The rainstorm intensity formula for the urban of Jingmen in Hubei province. Torr. Rain Disas. 35 (4), 386–391 (in Chinese with English abstract).
Kimoto, A., Nearing, M.A., Shipitalo, M.J., Polyakov, V.O., 2006. Multi-year tracking of sediment sources in a small agricultural watershed using rare earth elements. Earth Surf. Process. Landf. 31, 1763–1774.
Laflen, J.M., Lwonard, J.L., Foster, G.R., 1991. WEPP a new generation of erosion prediction technology. J. Soil Water Conserv. 46, 34–38.
Le Bissonnais, Y., 1996. Aggregate stability and assessment of soil crustability and erodibility: I. Theory and methodology. Eur. J. Soil Sci. 47, 425–437.
Le Bissonnais, Y., Arrouays, D., 1997. Aggregate stability and assessment of soil crustability and erodibility: application to humic loamy soils with various organic carbon contents. Eur. J. Soil Sci. 48, 39–48.
Le Bissonnais, Y., Blavet, D., De Noni, G., Laurent, J.Y., Asseline, J., Chenu, C., 2007. Erodibility of Mediterranean vineyard soils: relevant aggregate stability methods and significant soil variables. Eur. J. Soil Sci. 58, 188–195.
Li, G., Abrahams, A.D., Atkinson, J.F., 1996. Correction factors in the determination of mean velocity of overland flow. Earth Surf. Process. Landf. 21, 509–515.
Liang, Y., Li, D.S., Lu, X.X., Yang, X., Pan, X.Z., Mu, H., Shi, D.M., Zhang, B., 2010. Soil

erosion changes over the past five decades in the red soil region of southern China. J. Mt. Sci-Engl. M 7, 92–99.
Liebenow, A.M., Elliot, W.J., Laflen, J.M., Kohl, K.D., 1990. Interrill erodibility: collection and analysis of data from cropland soils. Trans. ASAE 33, 1882–1888.
Liu, P.L., Tian, J.L., Zhou, P.H., Yang, M.Y., Shi, H., 2004. Stable rare earth element tracers to evaluate soil erosion. Soil Tillage Res. 76, 147–155.
Liu, G., Yang, M.Y., Warrington, D.N., Liu, P.L., Tian, J.L., 2011. Using beryllium-7 to monitor the relative proportions of interrill and rill erosion from loessal soil slopes in a single rainfall event. Earth Surf. Process. Landf. 36, 439–448.
Liu, G., Xiao, H., Liu, P.L., Zhang, Q., Zhang, J.Q., 2016a. Using rare earth elements to monitor sediment sources from a miniature model of a small watershed in the Three Gorges area of China. Catena 143, 114–122.
Liu, G., Xiao, H., Liu, P.L., Zhang, Q., Zhang, J.Q., 2016b. An improved method for tracing soil erosion using rare earth elements. J. Soils Sediments 16 (5), 1670–1679.
Mabit, L., Benmansour, M., Walling, D.E., 2008. Comparative advantages and limitations of the fallout radionuclides ^{137}Cs, $^{210}Pb_{ex}$ and ^{7}Be for assessing soil erosion and sedimentation. J. Environ. Radioact. 99, 1799–1807.
Mahler, B.J., Philip, B.C., Zimmerman, M., 1998. Lanthanide-labeled clay: a new method for tracing sediment transport in Karst. Ground Water 36, 835–842.
Matisoff, G., Ketterer, M.E., Wilson, C.G., Layman, R., Whiting, P.J., 2001. Transport of rare earth element-tagged soil particles in response to thunderstorm runoff. Environ. Sci. Technol. 35, 3356–3362.
Mbagwu, J.S.C., Auerswald, K., 1999. Relationship of percolation stability of soil aggregates to land use, selected properties, structural indices and simulated rainfall erosion. Soil Tillage Res. 50, 197–206.
Nachtergaele, J., Poesen, J., 1999. Assessment of soil losses by ephemeral gully erosion using high-altitude (stereo) aerial photographs. Earth Surf. Process. Landf. 4, 693–706.
Nearing, M.A., Foster, G.R., Lane, L.J., 1989. A process-based soil erosion model for USDA-water erosion prediction project technology. Trans. ASAE 32, 1587–1593.
Polyakov, V.O., Nearing, M.A., 2004. Rare earth element oxides for tracing sediment movement. Catena 55, 255–276.
Polyakov, V.O., Kimoto, A., Nearing, M.A., Nichols, M.H., 2009. Tracing sediment movement on a semiarid watershed using Rare Earth Elements. Soil Sci. Soc. Am. J. 73, 1559–1565.
Shi, Z.H., Yan, F.L., Li, L., Li, Z.X., Cai, C.F., 2010. Interrill erosion from disturbed and undisturbed samples in relation to topsoil aggregate stability in red soils from subtropical China. Catena 81, 240–248.
Shi, Z.H., Fang, N.F., Wu, F.Z., Wang, L., Yue, B.J., Wu, G.L., 2012. Soil erosion processes and sediment sorting associated with transport mechanisms on steep slopes. J. Hydrol. 454–455, 123–130.
Six, J., Bossuyt, H., Degryze, S., Denef, K., 2004. A history of research on the link between (micro) aggregates, soil biota, and soil organic matter dynamics. Soil Tillage Res. 79, 7–31.
Soil Survey Staff, 2014. Keys to Soil Taxonomy, 12th ed. USDA—United States Department of Agriculture, Natural Resources Conservation Service, Washington, DC.
Song, W., Liu, P.L., Yang, M.Y., Xue, Y.Z., 2003. Using REE tracers to measure sheet erosion changing to rill erosion. J. Rare Earths 21, 587–590.
Stefano, D.C., Ferro, V., Pampalone, V., Sanzone, F., 2013. Field investigation of rill and ephemeral gully erosion in the Sparacia experimental area, South Italy. Catena 101, 226–234.
Stefanovic, J.R., Bryan, R.B., 2009. Flow energy and channel adjustments in rills developed in loamy sand and sandy loam soils. Earth Surf. Process. Landf. 34, 133–144.
Tian, J.L., Zhou, P.H., Liu, P.L., 1994. REE tracer method for studies on soil erosion. Int. J. Sediment Res. 9, 39–46.
Truman, C.C., Bradford, J.M., 1995. Laboratory determination of interrill soil erodibility. Soil Sci. Soc. Am. J. 59, 519–526.
USEPA, 1995. Test Methods for Evaluating Solid Waste-SW864, Update III, third ed. US Gov. Print. Office, Washington, DC.
Valmis, S., Dimoyiannis, D., Danalatos, N.G., 2005. Assessing interrill erosion rate from soil aggregate instability index, rainfall intensity and slope angle on cultivated soils in central Greece. Soil Tillage Res. 80, 139–147.
Wang, N., Yang, C.Y., Zhang, G., Xu, P.Z., Zou, T.T., 2008. Soil erosion of soil REE tracer study. Sci. Geogr. Sin. 28, 565–570 (in Chinese with English abstract).
Wang, J.G., Li, Z.X., Cai, C.F., Yang, W., Ma, R.M., Zhang, G.B., 2012. Predicting physical equations of soil detachment by simulated concentrated flow in Ultisols (subtropical China). Earth Surf. Process. Landf. 37, 633–641.
Wang, B., Zheng, F.L., Römkens, M.J.M., Darboux, F., 2013. Soil erodibility for water erosion: a perspective and Chinese experiences. Geomorphology 187, 1–10.
Wang, J.G., Yang, W., Yu, B., Li, Z.X., Cai, C.F., Ma, R.M., 2016. Estimating the influence of related soil properties on macro- and micro-aggregate stability in ultisols of south-central China. Catena 137, 545–553.
Wirtz, S., Seeger, M., Remke, A., Wengel, R., Wagner, J.F., Ries, J.B., 2013. Do deterministic sediment detachment and transport equations adequately represent the process-interactions in eroding rills? An experimental field study. Catena 101, 61–78.
Xue, Y.Z., Liu, P.L., Yang, M.Y., Ju, T.J., 2004. Study of spatial and temporal processes of soil erosion on sloping land using rare earth elements as tracers. J. Rare Earths 22, 707–713.
Yan, F.L., Shi, Z.H., Li, Z.X., Cai, C.F., 2008. Estimating interrill soil erosion from aggregate stability of Ultisols in subtropical China. Soil Tillage Res. 100, 34–41.
Yang, M.Y., Walling, D.E., Tian, J.L., Liu, P.L., 2006. Partitioning the contributions of sheet and rill erosion using beryllium-7 and cesium-137. Soil Sci. Soc. Am. J. 70, 1579–1590.
Young, R.A., Holt, R.F., 1968. Tracing soil movement with fluorescent glass particles. Soil Sci. Soc. Am. J. 32, 600–602.
Zhang, B., Horn, R., 2001. Mechanisms of aggregate stabilization in Ultisols from subtropical China. Geoderma 99, 123–145.
Zhang, X.C., Friedrich, J.M., Nearing, M.A., Norton, L.D., 2001. Potential use of rare earth oxides as tracers for soil erosion aggregation studies. Soil Sci. Soc. Am. J. 65, 1508–1515.
Zhang, G.H., Liu, B.Y., Liu, G.B., He, X.W., Nearing, M.A., 2003. Detachment of undisturbed soil by shallow flow. Soil Sci. Soc. Am. J. 67, 713–719.
Zhang, G.H., Luo, R.T., Cao, Y., Shen, R.C., Zhang, X.C., 2010. Correction factor to dye-measured flow velocity under varying water and sediment discharges. J. Hydrol. 389, 205–213.
Zheng, F.L., Tang, K.L., Zhou, P.H., 1989. Study on factors affecting rill erosion on cultivated slope land. Acta Pedol. Sin. 26, 109–116 (in Chinese with English abstract).
Zhu, Y.M., Tan, S.D., Dang, H.S., Zhang, Q.F., 2011. Rare earth elements tracing the soil erosion processes on slope surface under natural rainfall. J. Environ. Radioact. 102, 1078–1084.